Investigation of particle-unbound excited states in light nuclei with resonance-decay spectroscopy using a ^{12}Be beam

R. J. Charity, S. A. Komarov, and L. G. Sobotka
Departments of Chemistry and Physics, Washington University, St. Louis, Missouri 63130, USA

J. Clifford, D. Bazin, A. Gade, Jenny Lee, S. M. Lukyanov,* W. G. Lynch, M. Mocko, S. P. Lobastov,*
A. M. Rogers, A. Sanetullaev, M. B. Tsang, M. S. Wallace, and R. G. T. Zegers
National Superconducting Cyclotron Laboratory and Department of Physics and Astronomy
Michigan State University, East Lansing, Michigan 48824, USA

S. Hudan and C. Metelko
Department of Chemistry and Indiana University Cyclotron Facility, Indiana University, Bloomington, Indiana 47405, USA

M. A. Famiano and A. H. Wuosmaa
Department of Physics, Western Michigan University, Kalamazoo, Michigan 49008, USA

M. J. van Goethem
Kernfysisch Versneller Institut, NL-9747 AA Groningen, The Netherlands
(Received 2 September 2008; published 10 November 2008)

Resonance-decay spectroscopy is used to study particle-unbound excited states produced in interactions of $E/A = 50$ MeV ^{12}Be on polyethylene and carbon targets. The particle-unbound states are produced in a variety of reaction mechanisms, ranging from projectile fragmentation to proton pickup. New proton-decaying excited states are observed in ^{9}Li($E^* = 14.1 \pm 0.1$ MeV, $\Gamma = 207 \pm 49$ keV) and ^{10}Be($E^* = 20.4 \pm 0.1$ MeV, $\Gamma = 182 \pm 74$ keV). In addition a new α-decaying state is observed in ^{13}B($E^* = 13.6 \pm 0.1$ MeV, $\Gamma \leqslant 320$ keV). Also found was a ^{8}Be state with $E^* = 23$ MeV, $\Gamma = 616 \pm 30$ keV, which decays to the $p + {}^{3}\mathrm{H} + \alpha$ channel. Correlation between the fragments indicates that the decay is initiated by a proton emission to the 4.63-MeV state of ^{7}Li and the spin of the state is $J > 2$. A second $T = 2$ state was confirmed in ^{12}B at 14.82 MeV, which decays to the $p + {}^{11}\mathrm{Be}$, $^{3}\mathrm{H} + {}^{9}\mathrm{Be}$, and $\alpha + {}^{8}\mathrm{Li}$ channels. Its width was found to be $\Gamma \leqslant 100$ keV and its spin is consistent with $J^\pi = 2^+$.

DOI: 10.1103/PhysRevC.78.054307 PACS number(s): 21.10.−k, 25.70.Ef, 25.60.−t, 27.20.+n

I. INTRODUCTION

Particle-unstable states can be experimentally studied by using resonance-decay spectroscopy [1,2]. By detecting the decay products and their relative velocities, the excitation energy of the initial state can be deduced from the invariant mass. An alternative to resonance-decay spectroscopy is to produce the excited state in pickup, transfer, and other reactions where there are two reaction products after the initial collision. From the measured angle and the energy of any one of these products, the excitation energy can be deduced via two-body kinematics. Resonance-decay spectroscopy has one advantage over this more standard method in that the excitation-energy resolution is independent of the reaction kinematics. Therefore it can be used with poor-quality beams where the beam divergence and its energy spread are large. Large beam sizes can also be tolerated because, although these give rise to uncertainties in the measured absolute scattering angles, the relative angles of the decay products are unchanged to first order. In addition, resonance-decay spectroscopy can also be used in fragmentation reactions where there are more than two reaction products and the kinematics of any one fragment does not give information on the excitation energy.

Resonance-decay spectroscopy therefore has advantages when using exotic beams produced at fragmentation facilities where the secondary beam quality is poor. The large beam energies typically used with fragmentation reactions allow for the use of thick targets with the major limitation being the small-angle scattering of the decay products as they leave the target. However, the requirement of detecting all the decay fragments can lead to reduced efficiencies especially if there are more than two fragments. To overcome this limitation, large detector arrays covering most of the available phase space are advantageous. In this work the HiRA array [3] is used.

For neutron-rich nuclei, the thresholds for charge-particle decay are large and therefore charge-particle exit channels only access states at high excitation energy where the levels are typically wide and the level spacing is small. In particular, the phase space available for neutron decay is large and hence the branching ratio for these charge-particle exit channels will generally be small. Therefore the observation of any narrow state in these charged-particle decay channels will signal the presence of an unusual nuclear structure that suppresses

*On leave from Flerov Laboratory of Nuclear Reactions, Joint Institute for Nuclear Research, RU-141980 Dubna, Moscow region, Russian Federation.

neutron emission. As an example, high-T states suppress neutron emission owing to isospin conservation. Such states are often seen in proton-decay channels, which conserve isospin. Alpha-decay channels are also known to preferentially select out α-cluster states, such are molecular resonances, especially for energies just above the α-decay threshold [4].

In this study we report on particle-unstable excited states produced with a secondary, neutron-rich $E/A = 50$ MeV ^{12}Be beam interacting on polyethylene and carbon targets. Charged-particle decay channels were observed for a variety of Li, Be, and B isotopes produced in reactions ranging from pickup to fragmentation. The experimental apparatus is described in Sec. II and the results for each of the isotopes are given in Sec. III. Results for ^{12}Be excited states have already been presented in Ref. [5] and thus will not be discussed in this work. Finally, the conclusions of this study are presented in Sec. IV.

II. EXPERIMENTAL METHOD

A primary beam of $E/A = 120$ MeV ^{18}O was extracted from the Coupled Cyclotron Facility at the National Superconducting Cyclotron Laboratory at Michigan State University. This beam bombarded a ^{9}Be target, and ^{12}Be projectile-fragmentation products were selected by the A1900 separator. The secondary ^{12}Be beam, with intensity of 1×10^5 s^{-1}, purity of 87%, and momentum acceptance of $\pm 0.5\%$, impinged on targets of polyethylene and ^{12}C with thicknesses of 1.0 and 0.4 mm, respectively, located at the end of the S800 analysis beam line. The beam spot on these targets was approximately 1 cm $\times$ 2 cm in area. Event-by-event time of flight was used to reject the beam contaminants.

Charged particles produced in the reaction were detected in the HiRA array, [3] which consisted of 16 E-ΔE [Si-CsI(Tl)] telescopes located 60 cm downstream of the target. The telescopes were arranged in four towers of four telescopes each, with two towers on each side of the beam. The array subtended the angular region $2.7^\circ < \theta < 24.8^\circ$. Each telescope consisted of a 1.5-mm-thick, double-sided Si strip ΔE detector followed by a 4-cm-thick CsI(Tl) E detector. The ΔE detectors are 6.4 cm $\times$ 6.4 cm in area with the faces divided into 32 strips. Each E detector consisted of four separate CsI(Tl) elements, each spanning a quadrant of the preceding Si detector. Signals produced in the 1024 Si strips were processed with the HINP16C chip electronics [6]. More details of the setup, the energy calibration of the detectors, and the energy and particle-identification resolution can be obtained from Ref. [5].

III. RESULTS

Particle-unbound excited states can be found from the correlations between the decay products. The excitation energy is reconstructed from the kinetic energy of these fragments in their center-of-mass frame after the decay Q value is subtracted. In the following, we present excitation-energy distributions obtained from pairs and, in some cases, triplets of particles detected in coincidence. Peaks observed in these distributions will be compared to the compiled levels in Refs. [7–10]. In some cases new levels are observed. Results will be displayed for the polyethylene target, unless otherwise specified. However, most peaks visible in these spectra are also present in the data obtained with the C target. Table I lists the properties of states in this work for which new information is determined.

TABLE I. The excitation energy, width, spin, and isospin of states for which new information is determined.

Nucleus	Decay	E^* (MeV)	Γ (keV)	J^π	T
^{9}Li	p	14.1 ± 0.1	207 ± 49	$(1/2^+)$	(5/2)
^{8}Be	p	23.0 ± 0.1	616 ± 30	$\geqslant 3$	(1)
^{9}Be	p	18.54 ± 0.05	432 ± 50		(3/2)
^{10}Be	p	20.4 ± 0.1	182 ± 74	$(1/2^+)$	(2)
^{12}B	α	12.74 ± 0.05	$\leqslant 40$	0^+	2
^{12}B	α, p, ^{3}H	14.82 ± 0.05	$\leqslant 100$	2^+	2
^{13}B	α	13.6 ± 0.1	$\leqslant 320$		

To obtain widths and cross sections for the new levels, Monte Carlo simulations were preformed to estimate the experimental excitation-energy resolution and detection efficiency. These include the effects of the beam-spot size, energy loss [11], small-angle scattering in the target [12] and the angular and energy resolution of the detector array. These simulations are discussed in more detail in Ref. [5], where they are shown to be accurate for a number of known narrow levels.

A. Li isotopes

Lithium excited states are observed in the d-α and ^{3}H-α correlations in Figs. 1(a) and 1(b). The correlations are well known and are associated with the 3^+, 2.186-MeV, first excited state of ^{6}Li and the $7/2^-$, 4.63-MeV, second excited state of ^{7}Li. At a much lower intensity, one can see contributions from the wider 6.68- and 7.45-MeV states in ^{7}Li. Proton-decaying states are also observed for ^{7}Li and ^{9}Li in Figs. 1(b) and 1(c). The $3/2^-$, 11.24-MeV state of ^{7}Li, which is prominent in the p-^{6}He correlations, is the first $T = 3/2$ state in ^{7}Li. The 14.15 ± 0.05 MeV peak present in the p-^{8}He correlations [Fig. 1(c)] is previously unknown. The width of this peak is FWHM = 221 keV and after correcting for the simulated resolution (74 keV) we obtain $\Gamma = 207 \pm 49$ keV.

Rogachev *et al.* have searched for higher lying $T = 5/2$ states from the excitation function of $p + {}^{8}$He elastic scattering using the thick-target inverse kinematic method [13]. The present $p + {}^{8}$Li resonance is below their low-energy threshold and thus was not observed. One should consider whether the new 14.15-MeV state is $T = 5/2$, the isobaric analog of ^{9}He. The ground state of ^{9}He is claimed to be a virtual $n(1s_{1/2})$-^{8}He resonance with the pole of the S matrix almost at threshold [14]. The locations of the $0p_{1/2}$ and $1s_{1/2}$ neutron orbitals are already inverted for ^{11}Be and so a neutron in the $1s_{1/2}$ orbit is expected for the ground state of ^{9}He. Unlike ^{11}Be, the virtual nature of this resonance implies it is unbound.

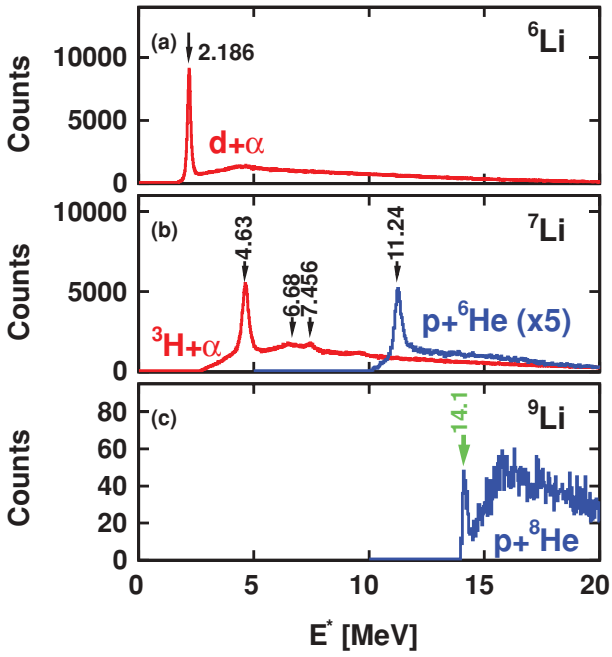

FIG. 1. (Color online) Experimental excitation-energy distributions for (a) ^{6}Li fragments from d-α correlations, (b) ^{7}Li fragments from ^{3}H-α and p-^{6}He correlations, and (c) ^{9}Li fragments from p-^{8}He correlations. In this and subsequent figures, levels discussed in the text are indicated by the arrows, which are labeled by the excitation energy in MeV. New, previously unknown, levels are indicated by the larger arrows. For display purposes, the $p + {}^6$He curve has been scaled by the indicated factor.

For the 14.15-MeV state to be the analog of this virtual state, the Coulomb displacement energy would then be ∼0.22 MeV. This is unusually small compared to the values of 0.84, 0.82, and 0.95 MeV for the isobaric analogs of ^{6}He, ^{7}He, and ^{8}He, respectively. Such a small Coulomb displacement energy for a $J = 1/2^+$ state could be interpreted as a Thomas-Ehrman shift [15,16]. For example, one sees a shift of 730 keV in the excitation energies of the $J = 1/2^+$, first excited states of ^{13}N and ^{13}C [15,16]. In addition, for ^{15}N, the Coulomb displacement energy for the isobaric analog of ^{15}C($J = 1/2^+$) is 2.52 MeV. This is small compared to the value of 3.53 MeV for the isobaric analog of ^{15}N($J = 1/2^-$) in ^{15}O. In these examples, both the ^{13}C and ^{15}C $J = 1/2^+$ states are particle bound. However, for the unbound $J = 1/2^+$ first-excited states in ^{9}B and ^{9}Be, Barker argues for an inverted Thomas-Ehrman shift [17].

The sign of the Thomas-Ehrman shift for a virtual unbound state is not clear; in fact the concept of the analog of a virtual state may be troublesome. If we consider the ^{9}He ground-state configuration as a $^8\text{He} \times \nu(1s_{1/2})$ virtual resonance, then the isobaric analog will be $\frac{1}{\sqrt{5}}{}^8\text{He} \times \pi(1s_{1/2}) + \frac{1}{\sqrt{5}}{}^8\text{Li}^{\text{IAS}} \times \nu(1s_{1/2})$, where $^8\text{Li}^{\text{IAS}}$ is the isobaric analog of the ^{8}He ground state. If the second term is also a virtual resonance, then one cannot ascribe the analog state in ^{9}Li as a normal resonance with a width and a wave function that is localized in the vicinity of the nucleus.

B. ^{8}Be decay

The excitation-energy distribution derived from α-α coincidences shown in Fig. 2(a) and 2(b) contains some well-known features. At low-excitation energy [Fig. 2(a)] we see the narrow ground state and the wide 2^+, 3.03-MeV, first excited state of ^{8}Be. In between there is another peak, which is not produced from ^{8}Be decay. Instead, it is associated with three-body decay of the 2.43-MeV state in ^{9}Be to the $n + 2\alpha$ channel [18].

At higher excitation energies [Fig. 2(b)] the $\alpha + \alpha$ channel has a peak that probably has contributions from both the 16.626- and 16.922-MeV states of ^{8}Be. Both of these $J^\pi = 2^+$ states have strong isospin mixing ($T = 0$ and $T = 1$). The $p + {}^7$Li exit channel has peaks associated with the 1^+, 17.64-MeV analog state and the 1^+, 18.15-MeV, $T = 0$ state. A third wider peak is present in the $p + {}^7$Li data at ∼19 MeV. This peak may have contributions from the 2^-, 18.91-MeV, the 3^+, 19.07-MeV, and the 3^+, 19.24-MeV states.

The three-body exit channel $\alpha + {}^3\text{H} + p$ also shows the presence of a peak structure at 23.0 ± 0.1 MeV in Fig. 2. The dashed histogram in Fig. 2 shows the equivalent distribution when the excitation energy of the $^3\text{H} + \alpha$ pair is gated on the peak associated with the $J = 7/2^-$, 4.63-MeV state of ^{7}Li in Fig. 1(b). This gate maintains the 23-MeV peak but suppresses the background. Thus the decay of this state can be considered as two sequential binary decays: an initial proton decay to the 4.63-MeV state of ^{7}Li, which subsequently decays into a

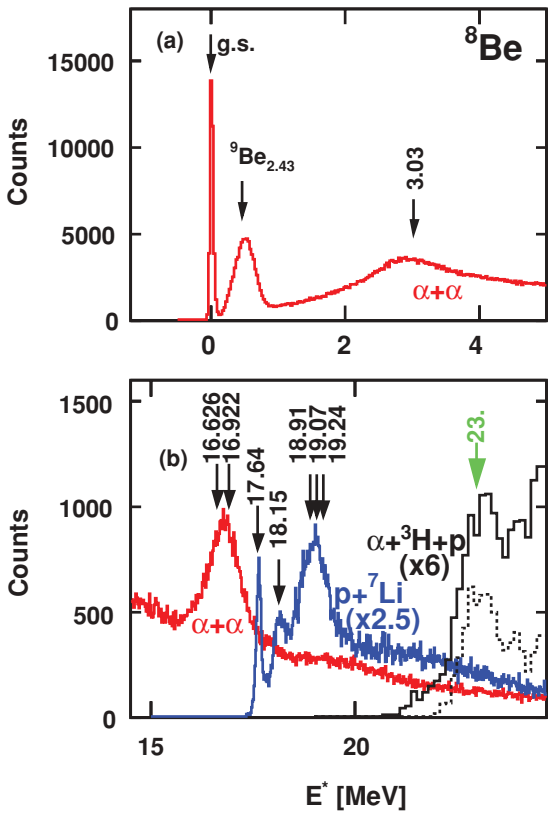

FIG. 2. (Color online) Experimental excitation-energy distributions of ^{8}Be fragments from α-α, p-^{7}Li, and p-^{3}H-α correlations. The dashed histograms indicate the p-^{3}H-α distribution after gating on the 4.63-MeV state in the ^{3}H-α channel.

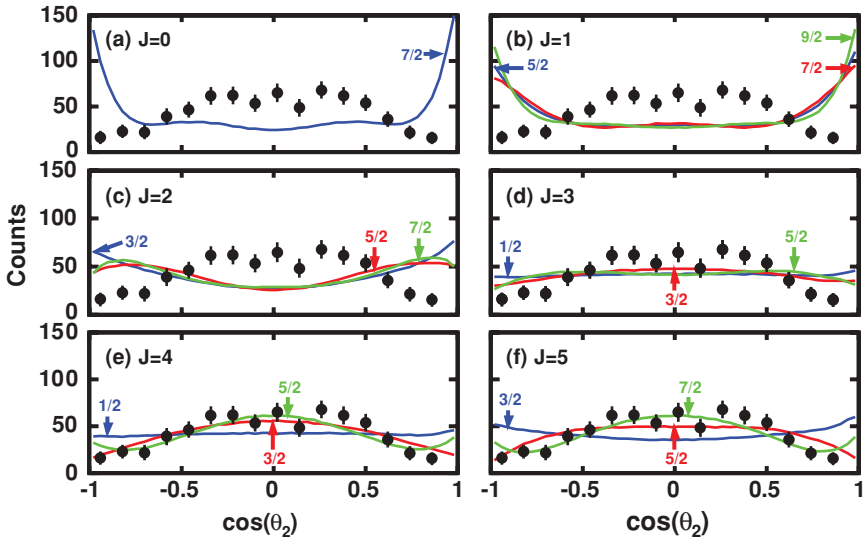

FIG. 3. (Color online) Distribution of the cosine of the relative angle between the two decay steps associated with the 23.0-MeV state in ^{8}Be. In each panel, the data points show the experimental angular distribution. Each panel shows the predictions for the indicated angular momentum (J) of the initial state. Different curves correspond to the indicated total angular momentum j removed by the proton.

triton-α pair. The experimental width of this peak is FWHM = 690 keV, and given the simulated experimental resolution of 310 keV, we find $\Gamma = 616 \pm 30$ keV. Ajzenberg-Selove *et al.* have already found a ^{8}Be state at 22.98 ± 0.1 MeV [19]; however, this must be a separate state as their experimental width is $\Gamma \leqslant 0.3$ MeV, inconsistent with our result.

Information about the spin of this state can be obtained from the angular correlations between the two decay steps (i.e., the relative angle θ_2 between the emission angle of the proton and the α-^{3}H decay axis). The data points in Fig. 3 show the experimental $\cos(\theta_2)$ correlations in the ^{8}Be center-of-mass frame. The experimental distribution, plotted in each panel, was obtained from the combined data collected with both the polyethylene and carbon targets, where a gate on the ^{3}H-α correlation has been applied and the background subtracted. The ^{7}Li intermediate state has a spin of $7/2^{-}$ and therefore the orbital angular momentum in the ^{3}H-α decay is $\ell = 3$. The possible orbital angular momenta of the emitted proton depend on the spin of the initial state, but angular-momentum conservation implies restrictions on the relative orientations of the two orbital-angular-momentum vectors, which give rise to correlations between the emission angles in the two decay steps. A full quantum treatment of this can be found in Refs. [20,21]. The curves in Figs. 3(a)–3(f) show predicted correlations assuming initial spins from 0 to 5, respectively. In each panel, the curves are labeled by j, the total angular momentum removed by the proton. Only the predictions for the lowest three pure values of j are shown in Figs. 3(c)–3(f). Higher j values are less probable owing to the higher centrifugal barrier and, in any case, they deviate more from the experimental data.

In addition to the angular correlations determined from Refs. [20,21], we have used the Monte Carlo simulations to include the detector response. The detector bias is generally minor. As a example for $j = 1/2$ ($J = 3, 4$) decay, the decay axes are uncorrelated and thus the predicted distributions should be flat without detector response. Therefore the small deviations from this behavior are due to detector bias. Note that the angular correlations are not sensitive to the parity of the initial state. Therefore, a 4^{+} state in which the proton has $j = 3/2, \ell = 2$ has the same correlations as a 4^{-} state where the proton has $j = 3/2, \ell = 1$. From a comparison of the predictions in Fig. 3 with the experimental data, it is clear that initial spins of $J < 4$ are not possible if the proton has a pure value of j.

For superpositions of j values, intermediate correlations are not necessarily obtained as there is an interference term. For $J = 3$, with a highly mixed $j = 3/2, 5/2$ configuration it was found possible to reproduce the experimental correlation. However, for lower spins, no admixtures of j values provided a good fit. Therefore it is concluded that the spin of this ^{8}Be state is $J \geqslant 3$. This proton-decaying 23.0-MeV state therefore is a candidate for the analog of the narrow 6.53-MeV, $J = 4^{+}$, $\Gamma = 35$ keV state in ^{8}Li.

C. ^{9}Be decay

Excitation-energy distributions from p-^{8}Li and d-^{7}Li correlations are shown in Fig. 4. In both spectra, small peaks associated with the $1/2^{-}$, 16.98-MeV, $T = 3/2$ analog state are visible. This state decays predominantly by neutron and α emission, which we cannot observe. Note that α decay leads to ^{5}He, which is neutron unstable and thus not observable in this work. A peak associated with the 17.495-MeV state is visible for the $d + ^{7}$Li channel. A very prominent peak is observed in the $p + ^{8}$Li channel at $E^{*} = 18.54 \pm 0.05$ MeV with a FWHM of 470 keV. By accounting for the detector resolution, the intrinsic width is 432 ± 50 keV. The prominence of this peak in the proton-decay channel suggests it is an analog state, possibly the analog of the $E^{*} = 4.296 \pm 0.015$ MeV, $\Gamma = 100 \pm 30$ keV state in ^{9}Li. However, the analog of this state is tentatively listed in the compilations at $E^{*} = 18.650 \pm 0.050$ MeV with $\Gamma = 300 \pm 100$ keV [10]. Within the quoted errors, both the energy and width are just consistent with the peak observed in this work. However, the compilations list an 18.58 ± 0.040 level of unknown width, which is also consistent with our peak location. This state is listed as having p, d, n, and α decay modes, but we see no evidence for it in the $d + ^{7}$Li exit channel.

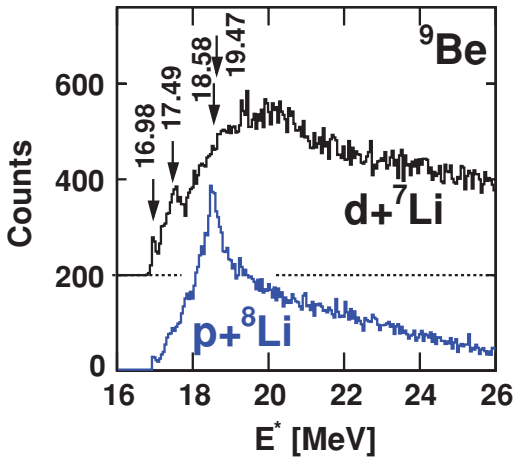

FIG. 4. (Color online) Excitation-energy distributions for ^{9}Be fragments determined from $p + {}^{8}$Li and $d + {}^{7}$Li correlations. For clarity, the $d + {}^{7}$Li results have been shifted upward along the y-axis.

D. ^{10}Be decay

^{10}Be states are seen in the excitation-energy distribution determined from α-^{6}He correlations in Fig. 5(a). The 2+, 9.64- and the 10.15-MeV states are clearly visible. Note that for the first peak we use the excitation energy of 9.64 MeV from Refs. [22,23] rather than the compiled value of 9.4 MeV. The 10.15-MeV state was recently found to be $J^{\pi} = 4^{+}$ and was interpreted as belonging to a highly deformed molecular band [24]. For $p + {}^{9}$Li correlations in Fig. 5(b), we observed a previously unknown state at 20.4 ± 0.1 MeV. Its experimental width is FWHM $= 296 \pm 8$ keV. Taking into account the simulated experimental resolution (130 keV) we find $\Gamma = 182 \pm 74$ keV. At higher excitation energies there is a broad structure in the $p + {}^{9}$Li data centered near 21.5 MeV. Within this structure there is indication of the 21.22-MeV state, which had tentatively been identified as a $J^{\pi} = 2^{-}, T = 2$ analog state [25]. However, there must be one or more unresolved states at higher excitation energies. These may be unknown higher lying analog states and there also may be a contribution from the known 21.8-MeV state.

The ground-state ^{10}Li has been reported to be a virtual state of a $1s_{1/2}$ neutron and ^{9}Li [26]. Could the new 20.4-MeV state be the analog of this virtual state? This is similar to our discussion of the relationship between the 14.1-MeV state in ^{9}Li to the proposed ^{9}He virtual ground state (Sec. III A). In both cases we are dealing with analogs of $N = 7$ nuclei, where the valance neutron occupies the $1s_{1/2}$ orbital. Like the previous discussion, the Coulomb displacement energy of ~0.66 MeV is small compared to values of 1.5 and 1.4 MeV for the analogs of ^{9}Li and ^{10}Li, respectively [27]. The structure of these two states may therefore be similar.

E. ^{10}B decay

The ^{10}B states observed from α and proton decay in Fig. 6(a) are all previously known. Three prominent peaks are found in the $\alpha + {}^{6}$Li distribution. Two of these peaks are associated with the 3^{+}, 4.774-MeV the 4^{+}, 6.025-MeV states.

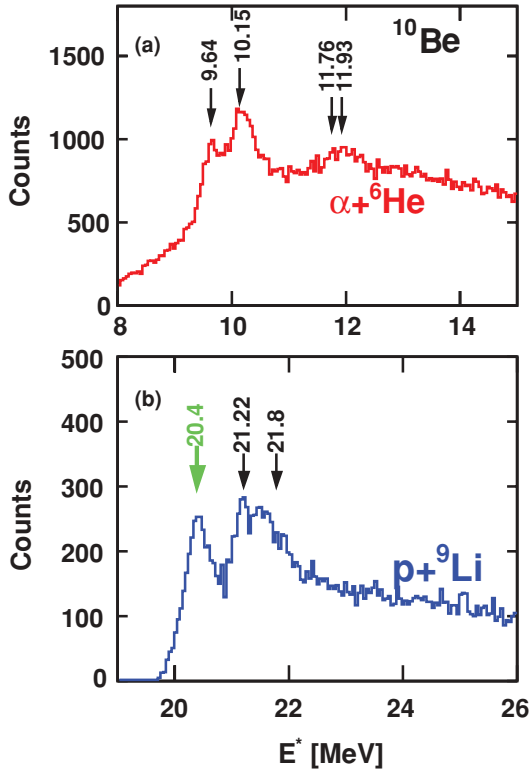

FIG. 5. (Color online) Experimental excitation-energy distributions for ^{10}Be fragments from (a) α-^{6}He and (b) p-^{9}Li correlations.

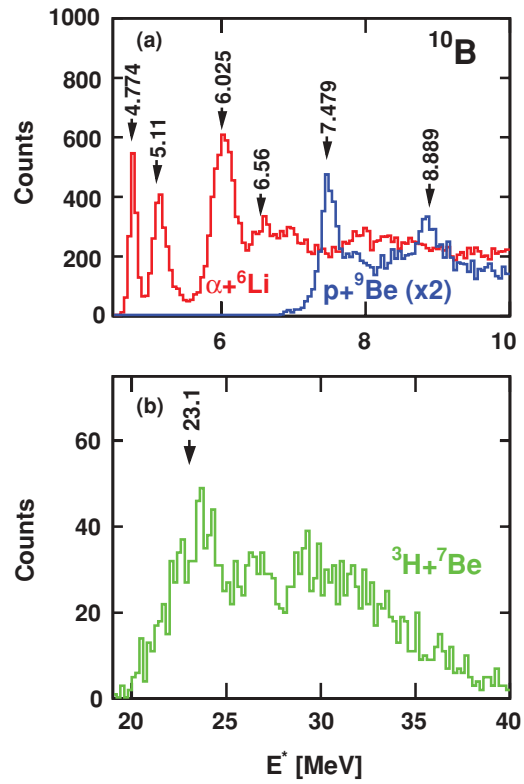

FIG. 6. (Color online) Experimental excitation-energy distributions of ^{10}B fragments from (a) α-^{6}Li and p-^{9}Be and (b) ^{3}H-^{7}Be correlations.

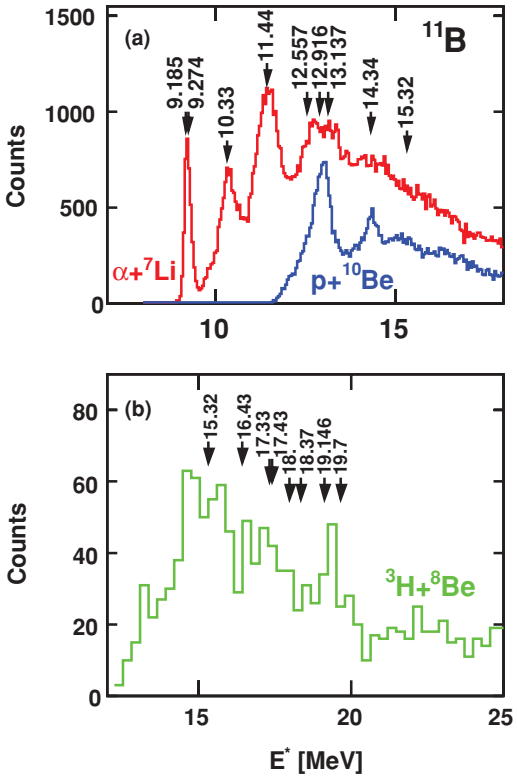

FIG. 7. (Color online) Experimental excitation-energy distributions of ^{11}B fragments from (a) α-^{7}Li and p-^{10}Be and (b) ^{3}H-^{8}Be correlations.

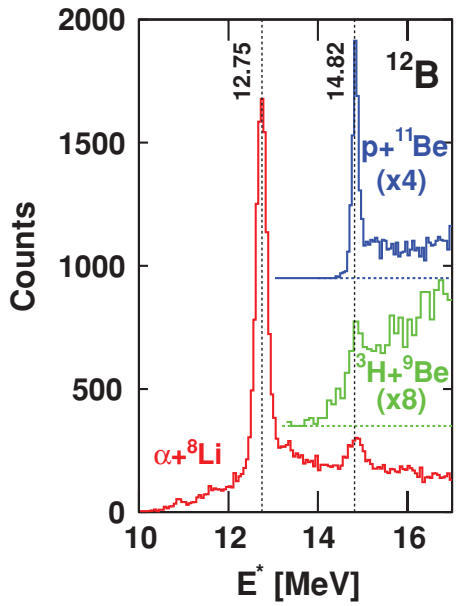

FIG. 8. (Color online) Experimental excitation-energy distributions of ^{12}B fragments determined from $\alpha + {}^{8}$Li, $p + {}^{11}$Be, and $^{3}\mathrm{H} + {}^{9}$Be exit channels. The results for the latter two channels have been shifted along the y-axis and scaled by the factors indicated in parentheses. The dashed lines indicate the location of known 12.75- and 14.82-MeV states.

The peak at 5.11 MeV may have contributions from a number of ^{10}B states. The 6.56-MeV state, although weakly present in the polyethylene data of Fig. 6(a), is more strongly populated in the data from the carbon target. The $p + {}^{9}$Be channel selects out the 2^{+}, 7.479-MeV and the 3^{-}, 8.889-MeV analog states. The excitation-energy distribution obtained from $^{3}\mathrm{H} + {}^{7}$Be pairs in Fig. 6(b) shows indications of a wide peak around 23 MeV and possibly other wide states at larger excitation. A broad 23.1-MeV peak has been observed previously.

F. ^{11}B decay

The excitation-energy spectra from α-^{7}Li correlations in Fig. 7(a) show four peaks, all of which can be associated with known ^{11}B excited states. The lowest energy peak probably has contributions from both the $7/2^{+}$, 9.18-MeV and $5/2^{+}$, 9.27-MeV states. The second and third peak can be associated with the $5/2^{-}$, 10.3-MeV and the 11.44-MeV states, respectively. Finally, the wider peak at approximately 13 MeV may have contributions from three known states, of 12.56, 12.916, and 13.14 MeV. As in other nuclei studied in this work, the proton-decay channel shown in Fig. 7(a) selects out high-isospin states. Peaks corresponding to $T = 3/2$ states at $E^{*} = 12.916$ MeV ($J^{\pi} = 1/2^{-}$) and $E^{*} = 14.34$ MeV($J^{\pi} = 5/2^{+}$) are clearly visible. There is evidence of the wide 15.32-MeV, $\Gamma = 635$ keV state, which was also been tentatively assigned as $T = 3/2$. There is also structure in the $^{3}\mathrm{H} + {}^{8}$Be excitation-energy distribution shown in Fig. 7(b); however, the statistical fluctuations are significant. This channel is constructed from $^{3}\mathrm{H} + \alpha + \alpha$ events with a suitable gate on the α-α relative energy to select out the ^{8}Be ground state [Fig. 2(a)]. There is a broad peak at $\sim$15 MeV located close to the previously mentioned 15.32-MeV $T = 3/2$ state. However, isospin considerations suggest the latter state contributes little to the $^{3}\mathrm{H} + {}^{7}$Be channel.

G. ^{12}B decay

For the polyethylene target, two ^{12}B levels are strongly populated in the excitation-energy distributions shown in Fig. 8. For the carbon target, these states are also seen but are very weakly populated. Thus most of the yield from the polyethylene target is associated with interactions on the hydrogen target nucleus through the $^{12}\mathrm{Be}(p, n)^{12}\mathrm{B}$ reaction. Such (p, n) reactions are known to preferentially populate analog states. In Fig. 8 the α-^{8}Li channel has a large peak at $E^{*} = 12.75$ MeV, which corresponds to the known 0^{+} isobaric analog state of ^{12}Be. This exit channel is isospin forbidden for a $T = 2$ level, but no isospin-allowed channels [e.g., $p + {}^{11}$Be or $n + {}^{11}\mathrm{B}^{*}$ ($T = 3/2$)] are energetically possible.

The cross section associated with α-^{8}Li channel for this state is 6.3 mb. The listed width of this state, 85 ± 40 keV [7], was taken from Ref. [28], in which the $^{9}\mathrm{Be}(^{7}\mathrm{Li}, \alpha)^{12}\mathrm{B}$ reaction was studied and a 12.77 ± 0.50-MeV peak (among many other states) was observed. However, this reaction is not expected to strongly populate analog states and, in fact, the authors of Ref. [28] were not certain that this 12.77-MeV level is an analog state. However, Barker [29] predicted the width of this state to be very small, on the order of a few keV.

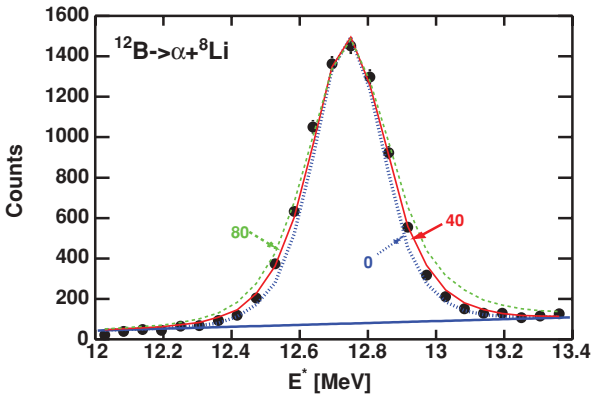

FIG. 9. (Color online) Excitation-energy distributions of ^{12}B fragments determined from the $\alpha + {}^{8}$Li exit channel. The points are the experimental data; the curves indicate the results of Monte Carlo simulations of the decay for the 12.75-MeV state assuming intrinsic widths of 0, 40, and 80 keV.

Experimentally, we find the FWHM of the 12.75-MeV $T = 2$ state in this work to be 290 keV, which is almost identical with the simulated resolution. Therefore it is possible that this state is very narrow, as predicted by Barker. Detailed simulations were performed with Breit-Wigner distributions, and by concentrating on the tails of the line shapes in Fig. 9, we determine that the intrinsic line width is $\leqslant$40 keV. This results suggests that the 12.75-MeV, $\Gamma = 85 \pm 40$ keV peak observed in Ref. [28] was a $T = 1$ state and not the isobaric analog state.

The known 14.82-MeV level is also observed in three exit channels in Fig. 8: $\alpha + {}^{8}$Li, $p + {}^{11}$Be, and ^{3}H + ^{9}Be. This state has been tentatively assigned as $T = 2$ and its strong population in (p, n) reactions confirms this assignment. Only the $p + {}^{11}$Be channel conserves isospin, but as this state is at the threshold for this channel (14.09 MeV) it will be suppressed by its small barrier penetration factor, possibly explaining the sizable branching to other isospin nonconserving channels. The width of this state is listed as $\leqslant$200 keV [7]. Experimentally, we obtained a FWHM of 153 keV from the peak in the $p + {}^{11}$Be channel, which has the largest signal-to-background ratio. This value is consistent with the simulated experimental resolution and thus we give a reduced limit for the width of $\Gamma \leqslant 100$ keV.

The joint velocity distributions of ^{12}B fragments determined for the two excited states are shown in Fig. 10. These distributions were obtained from the reconstructed ^{12}B velocity (the center-of-mass velocity of the detected decay products) after gating on the peaks in Fig. 8 and using the data from the carbon target to subtract the small contribution from interactions on the carbon component of the polyethylene target. In all cases the data lie close to the circles representing the expected loci for the ^{12}Be$(p, n)^{12}$B reaction, confirming this as the dominant reaction mechanism. The distributions along these loci are biased by the acceptance of the detector array.

The relative experimental angular distribution $(d\sigma/d\theta)$ of the reconstructed ^{12}B fragments in the reaction center-of-mass frame (hydrogen target) is plotted as the data points in Fig. 11 for the 12.75-MeV state. These data were obtained

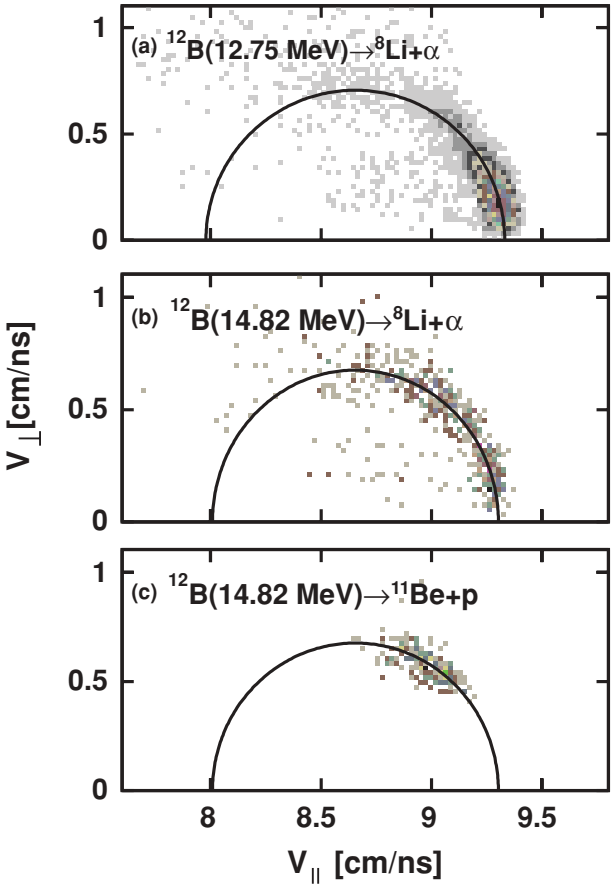

FIG. 10. (Color online) Experimental joint distributions of the parallel and perpendicular velocity components of ^{12}B parent fragments. (a) Results obtained for fragments in the 12.75-MeV excited state, which decay to the α-^{8}Li exit channel. Results for fragments in the 14.82-MeV states, which decay to (b) the $\alpha + {}^{8}$Li channel and (c) the $p + {}^{11}$Be channel. In each panel, the circle represents the expected loci for the ^{12}Be$(p, n)^{12}$B reaction.

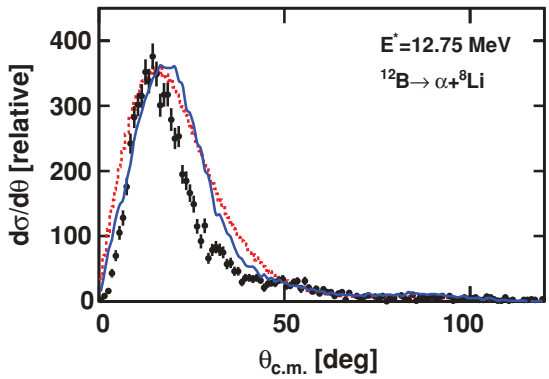

FIG. 11. (Color online) Relative angular distributions of ^{12}B fragments excited to the 12.75-MeV state in the center-of-mass frame for interactions with hydrogen target nuclei. The data points give the experimental distribution after the background from interaction with carbon target nuclei is subtracted. DWBA predictions are indicated by the dashed curve. The solid curve includes the effect of the detector acceptance.

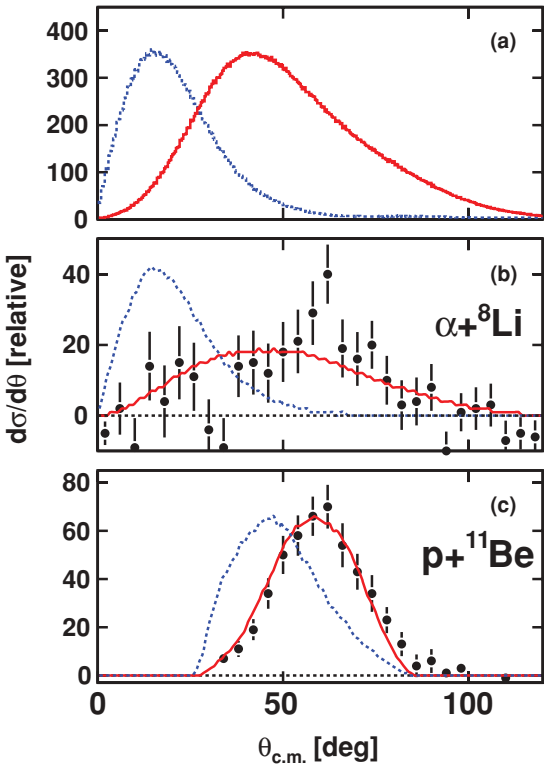

FIG. 12. (Color online) Relative angular distributions of ^{12}B fragments excited to the 14.82-MeV state in the center-of-mass frame for interactions with hydrogen target nuclei. (a) The solid curve is the predicted primary distribution for a 2^+ state. In comparison, the dashed curve shows the predicted distribution for the 0^+, 12.75-MeV state. In (b) and (c), distributions are shown for the $\alpha + {}^8$Li and $p + {}^{11}$Be exit channels, respectively. The data points are the experimental results after background subtraction. The dashed and solid curves are associated with the corresponding distribution in (a), but where the detector efficiency has been included.

from the $\alpha + {}^8$Li channel. For the 14.82-MeV state, equivalent distributions are plotted as data points in Figs. 12(b) and 12(c) for the $\alpha + {}^8$Li and $p + {}^{11}$Be channels, respectively. All these distributions have been corrected for background and interactions on the carbon target. The $p + {}^{11}$Be angular distribution in Fig. 12(c) is severely limited by the experimental acceptance of the ^{11}Be fragment, which makes up most of the mass of the parent ^{12}B fragment. This being the case, the velocity vector of this fragment is also approximately the reconstructed ^{12}B velocity vector. Center-of-mass angles below 30° are restricted owing to the angular acceptance of the detector array and angles above 80° are suppressed because of the low-energy threshold for ^{11}Be identification. For the $\alpha + {}^8$Li channel there are no severe acceptance problems and the simulated relative efficiencies for both levels have a similar dependence on the center-of-mass angle. Therefore, the differences in the $\alpha + {}^8$Li distributions for the two states in Figs. 11 and 12(b) reflect different primary angular distributions. The distribution for the 12.75-MeV state is strongly forward focused, consistent with its assignment as $J^\pi = 0^+$.

The 14.82-MeV state has been tentatively assigned $J^\pi = 2^+$ in the data base. However, Barker has suggested the possibility of $J^\pi = 0^+$ [29]. But as the angular distribution in Fig. 12(b) is less focused at small angles than the results for the $J^\pi = 0^+$, 12.75-MeV state (Fig. 11), this favors the original $J^\pi = 2^+$ assignment. To investigate this more quantitatively, we have compared the experimental data to DWBA calculations obtained from the code DW81 [30] using the effective nucleon-nucleon interaction of Love-Franey at 50 MeV [31]. Proton optical-model potentials were obtained from Fulmer *et al.* [32] and these were also used for neutrons. One-body transition densities were calculated with the code OXBASH [33] in the p shell by using the Cohen-Kurath II interaction [34]. Binding energies of particles were obtained with OXBASH using the SK20 interaction [35]. For $T = 2$ levels, the calculation predicts a 0^+ state at 13.67 MeV and a 2^+ state at 17.58 MeV. A second 0^+ state is not predicted until 29.94 MeV, so according to these calculation the second state should not be $J^\pi = 0^+$.

For the predicted 0^+ state, the angular distribution is shown as the curves in Fig. 11. The dashed curve gives the predicted DWBA distribution. The solid curve, where angular acceptance of the detector array has been included, should be compared to data. The agreement is moderately good, and the calculations reproduce the strong enhancement at forward angles. For the 14.82-MeV level, we have considered using both the predicted 0^+ and 2^+ angular distributions. These are compared in Fig. 12(a), where the dashed and solid curves are the 0^+ and 2^+ DWBA predictions, respectively. In Figs. 12(b) and 12(c), the corresponding distributions, including the detector acceptance, are shown by the curves. For both exit channels the predicted 2^+ distribution does a much better job at reproducing the experimental distribution than the 0^+ prediction. Thus we conclude that the 14.82-MeV state is not $J^\pi = 0^+$. The small width measured for this state also supports this conclusion [29].

Based on the $J^\pi = 2^+$ DWBA angular distributions, the total detection efficiency for the different exit channels of the 14.82-MeV state was determined. From these, the cross sections for the three observed branches are $522 \pm 150\ \mu$b($p + {}^{11}$Be), $190 \pm 57 \mu b(\alpha + {}^8$Li), and $59 \pm 17\ \mu$b(^{3}H + ^{9}Be).

A known 13.3-MeV state of ^{12}B is also observed in the $\alpha + {}^8$Li exit channel with the ^{12}C target (not shown).

H. ^{13}B decay

In this work, isolated low-energy ^{13}B excited states can only be assessed by reactions with carbon target nuclei. For interactions on hydrogen, ^{13}B represents the complete mass and charge in the reaction and thus, by energy conservation, the excitation energy deduced for all possible exit channels of ^{13}B decay will be the compound-nucleus excitation energy (~60 MeV) or slightly less if there is γ emission. This will be true irrespective of the reaction mechanism. Peaks corresponding to this excitation energy are observed in a large number of three-particle channels (e.g., $p + {}^3$H + ^{9}Li and $p + \alpha + {}^6$He). Any other peaks at much smaller excitation energies must derive from proton-pickup reactions with ^{12}C target nuclei. Figure 13 shows the excitation-energy distribution for ^{13}B fragments determined from α-^{9}Li correlations. Unlike previous figures, the data shown here are

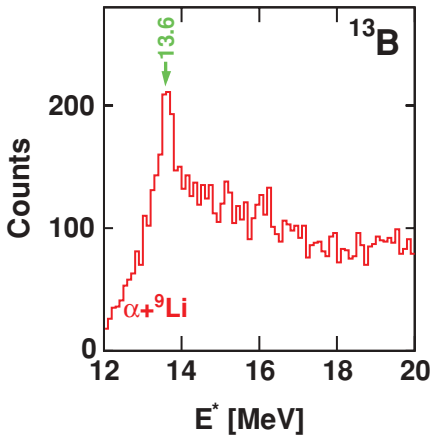

FIG. 13. (Color online) Excitation-energy distribution for ^{13}B fragments determined from α-^{9}Li correlations. A previously unknown level is indicated.

the combined data from the polyethylene and carbon targets as only carbon interactions are important. There are no previously known levels in the excitation region accessed by this channel and thus the prominent peak at 13.6 ± 0.1 MeV corresponds to a previously unknown state of ^{13}B. The experimental width is FWHM $= 406 \pm 49$ keV, and taking into account the simulated experimental resolution (320 keV) we find $\Gamma \leqslant$ 320 keV.

IV. CONCLUSIONS

Particle-unstable states in light nuclei have been investigated in interactions of $E/A = 50$ MeV ^{12}Be beam particles on polyethylene and carbon targets. Charge-particle exit channels were detected by using the HiRA array. Many known particle-unstable excited states in Li, Be, and B isotopes were observed. In addition, a number of new excited states were identified. These include a $E^* = 14.15 \pm 0.05$ MeV, $\Gamma = 207 \pm 49$ keV state in ^{9}Li and a $E^* = 20.4$ MeV, $\Gamma = 182 \pm 74$ keV state in ^{10}Be, both of which proton decay and may be analog states. In addition we see a $E^* = 13.6 \pm 0.1$ MeV, $\Gamma \leqslant$ 320 keV state in ^{13}B, which undergoes α decay. We have also observed a new state of ^{8}Be at $E^* = 23.0$ MeV, $\Gamma = 616 \pm 30$ keV. It was found to decay into three fragments (i.e., $p + {}^{3}\mathrm{H} + \alpha$). This decay consists of an initial proton decay to the $7/2^-$, 4.63-MeV state in ^{7}Li, which sequentially decays to a ^{3}H-α pair. From angular correlations, the spin of the initial state is restricted to $J \geqslant 3$, which suggests it might be the analog of the narrow 6.53-MeV, $J = 4^+$ state in ^{8}Li.

A second $T = 2$ state in ^{12}B at 14.82 MeV is confirmed and we obtained a new limit for its width of $\Gamma \leqslant 100$ keV. This state was formed in the ^{12}Be$(p, n)^{12}$B reaction and the angular distributions are consistent with the previously proposed $J^\pi = 2^+$ assignment. This state has decay branches to the $p + {}^{11}$Be, $\alpha + {}^{8}$Li, and ^{3}H + ^{9}Be exit channels with cross sections of 522 ± 150, 190 ± 57, and $59 \pm 17\,\mu$b, respectively. The 0^+, $T = 2$ level at $E^* = 12.75$ MeV was observed to have an α decay branch and its width is $\leqslant$40 keV.

ACKNOWLEDGMENTS

We would like to acknowledge useful discussions with F. C. Barker. This work was supported by the U.S. Department of Energy, Division of Nuclear Physics, under Grant Nos. DE-FG02-87ER-40316 and DE-FG02-04ER41320 and the National Science Foundation under Grant Nos. PHY-0606007 and PHY-9977707.

[1] D. Robson, Nucl. Phys. **A204**, 523 (1973).
[2] B. R. Fulton and W. D. M. Rae, J. Phys. G **16**, 333 (1990).
[3] M. S. Wallace *et al.*, Nucl. Instrum. Methods A **583**, 302 (2007).
[4] M. Freer and A. C. Merchant, J. Phys. G **23**, 261 (1997).
[5] R. J. Charity *et al.*, Phys. Rev. C **76**, 064313 (2007).
[6] G. L. Engel, M. Sadasivam, M. Nethi, J. M. Elson, L. G. Sobotka, and R. J. Charity, Nucl. Instrum. Methods A **573**, 418 (2007).
[7] F. Ajzenberg-Selove, Nucl. Phys. **A506**, 1 (1990).
[8] F. Ajzenberg-Selove, Nucl. Phys. **A523**, 1 (1991).
[9] D. R. Tilley, C. M. Cheves, J. L. Godwin, G. M. Hale, H. M. Hofmann, J. H. Kelley, C. G. Sheu, and H. R. Weller, Nucl. Phys. **A708**, 3 (2002).
[10] D. R. Tilley, J. H. Kelly, J. L. Godwin, D. J. Millener, J. E. Purcell, C. G. Sheu, and H. R. Weller, Nucl. Phys. **A745**, 155 (2004).
[11] J. F. Ziegler, J. P. Biersack, and U. Littmark, *The Stopping and Range of Ions in Solids* (Pergamon, New York, 1985). The code SRIM can be found at www.srim.org.
[12] R. Anne, J. Herault, R. Bimbot, H. Gauvin, C. Bastin, and F. Hubert, Nucl. Instrum. Methods B **34**, 295 (1988).
[13] G. V. Rogachev *et al.*, Phys. Rev. C **67**, 041603(R) (2003).
[14] L. Chen, B. Blank, B. A. Brown, M. Chartier, A. Galonsky, P. G. Hansen, and M. Thoennessen, Phys. Lett. **B505**, 21 (2001).
[15] J. B. Ehrman, Phys. Rev. **81**, 412 (1951).
[16] R. G. Thomas, Phys. Rev. **88**, 1109 (1952).
[17] F. C. Barker, Aust. J. Phys. **40**, 307 (1987).
[18] J. Pochodzalla *et al.*, Phys. Rev. C **35**, 1695 (1987).
[19] F. Ajzenberg-Selove, C. F. Maguire, D. L. Hendrie, D. K. Scott, and J. Mahoney, Phys. Rev. C **13**, 46 (1976).
[20] L. C. Biedenharn and M. E. Rose, Rev. Mod. Phys. **25**, 729 (1953).
[21] H. Frauenfelder, Annu. Rev. Nucl. Sci. **2**, 129 (1953).
[22] S. Hamada, M. Yasue, S. Kubono, M. H. Tanaka, and R. J. Peterson, Phys. Rev. C **49**, 3192 (1994).
[23] N. Soić *et al.*, Europhys. Lett. **34**, 7 (1996).
[24] M. Freer *et al.*, Phys. Rev. Lett. **96**, 042501 (2006).
[25] S. M. Abramovich, B. Ya. Guzhovshii, A. G. Zvenigorodskii, and S. V. Trusillo, Sov. J. Nucl. Phys. **30**, 665 (1979).
[26] M. Thoennessen *et al.*, Phys. Rev. C **59**, 111 (1999).
[27] T. Teranishi *et al.*, Phys. Lett. **B407**, 110 (1997).
[28] F. Ajzenberg-Selove, R. Middleton, and J. D. Garrett, Phys. Rev. C **12**, 1868 (1975).
[29] F. C. Barker, J. Phys. G **2**, L45 (1976).

[30] R. Schaeffer and J. Raynal, computer code DWBA70, SPtH, 1970 (unpublished); extended version DW81 by J. R. Comfort, University of Pittsburgh, 1981 (unpublished); updated version, 1986.
[31] M. A. Franey and W. G. Love, Phys. Rev. C **31**, 488 (1985).
[32] C. B. Fulmer, J. B. Ball, A. Scott, and M. L. Whiten, Phys. Rev. **181**, 1565 (1969).
[33] B. A. Brown, A. Etchegoyen, N. S. Godwin, W. D. M. Rae, W. A. Richter, W. E. Ormand, E. K. Warburton, J. S. Winfield, L. Zhao, and C. H. Zimmerman, Tech. Rep. MSU NSCL-1289, 2004.
[34] S. Cohen and D. Kurath, Nucl. Phys. **A101**, 1 (1967).
[35] B. A. Brown, Phys. Rev. C **58**, 220 (1998).